



**HAL**  
open science

# A homogenized micro-elastohydrodynamic lubrication model: Accounting for non-negligible microscopic quantities

Hugo Checo, David Dureisseix, Nicolas Fillot, Jonathan Raisin

## ► To cite this version:

Hugo Checo, David Dureisseix, Nicolas Fillot, Jonathan Raisin. A homogenized micro-elastohydrodynamic lubrication model: Accounting for non-negligible microscopic quantities. *Tribology International*, 2019, 135, pp.344-354. 10.1016/j.triboint.2019.01.022 . hal-02070567

**HAL Id: hal-02070567**

**<https://hal.science/hal-02070567>**

Submitted on 22 Oct 2021

**HAL** is a multi-disciplinary open access archive for the deposit and dissemination of scientific research documents, whether they are published or not. The documents may come from teaching and research institutions in France or abroad, or from public or private research centers.

L'archive ouverte pluridisciplinaire **HAL**, est destinée au dépôt et à la diffusion de documents scientifiques de niveau recherche, publiés ou non, émanant des établissements d'enseignement et de recherche français ou étrangers, des laboratoires publics ou privés.



Distributed under a Creative Commons Attribution - NonCommercial 4.0 International License

# A homogenized micro-elastohydrodynamic lubrication model: accounting for non-negligible microscopic quantities

Hugo M. Checo<sup>a,b</sup>, David Dureisseix<sup>a</sup>, Nicolas Fillot<sup>a,\*</sup>, Jonathan Raisin<sup>b</sup>

<sup>a</sup>Univ Lyon, INSA-Lyon, CNRS UMR5259, LaMCoS, F-69621, France

<sup>b</sup>Research Center of Solaize (CRES), Total Marketing Services, Solaize, France

---

## Abstract

In rough elastohydrodynamic lubricated contacts the geometry often exhibits two clearly separated scales: a macroscopic scale –the one of the bearing– and a microscopic scale, that of the surface roughness. In numerical simulation of lubricated contacts, this difference in scales leads to large systems of equations to solve. Assuming periodicity or pseudo-periodicity of the small scale, several methods to decouple the macro scale from the micro scale have been proposed, the formal approach being the homogenization theory. However, the approximation errors due to the classical asymptotic assumptions can be considerable. In this work we introduce a homogenized model which takes into account the non-negligible pressures and deformations of the micro scale, thus extending the applicability of the classical asymptotic homogenized approaches.

*Keywords:* homogenization, elastohydrodynamic lubrication, microelastohydrodynamic, roughness.

*2010 MSC:* 74F10, 76D08, 35B27, 41A60

---

\*Corresponding author

*Email address:* [Nicolas.Fillot@insa-lyon.com](mailto:Nicolas.Fillot@insa-lyon.com) (Nicolas Fillot )

---

**Nomenclature**

$h$	$H$	film thickness
$\delta$	$\Delta$	elastic body surface normal displacement
$l$	$\varepsilon, \varepsilon_0$	roughness wavelength
	$A$	roughness amplitude
$\xi$	$\xi$	roughness phase
$u_m$	$\bar{u}$	entrainment velocity
$W$		normal load per unit width
$\underline{\delta}$	$\underline{\Delta}$	displacement field in the equivalent solid
$p$	$P$	pressure
$\rho$	$\bar{\rho}$	fluid density
$\eta$	$\bar{\eta}$	fluid viscosity
$R$		equivalent curvature radius
$a$		contact half-width of Hertzian theory
$p_h$		maximum pressure of Hertzian theory
$\frac{\rho h^3}{12\eta}$	$\epsilon$	constitutive parameter
$x_1$	$X_1$	slow tangential spatial variable
	$Y_1$	fast tangential spatial variable
	$M, L$	Moes-Venner parameters

---

The symbol in the second column is the non-dimensional version of the one in the first column.

## 1. Introduction

Surface roughness has an impact on lubricated contacts, especially for those operating in severe conditions. Understanding the influence of the microgeometry of the surfaces in contact in the elastohydrodynamic (EHL) regime is essential for the design of improved bearings and mechanical transmissions. From the numerical point of view this constitutes a challenge, given the physics involved and the difference in scales imposed by the geometry of the bearing and the one of the surface roughness. This problem has been handled in two ways: a direct

resolution of the problem up to the microscopic scale, which is called in the  
10 literature the *deterministic* approach, and also by means of averaging methods.  
A recent paper by Pei et al [1] develops a deterministic multiscale computa-  
tional method (finite cell method, FCM) to solve rough lubricated contacts; it  
is however limited to conformal hydrodynamics contacts.

As pointed out by Gropper et al [2], direct simulation becomes too costly  
15 for state of the art simulations of EHL contacts, and thus it is restricted to very  
small domains, such as Hertzian contacts. State of the art modeling involves  
non-Newtonian fluids, thermal (TEHL) and piezoviscous effects as well as solid  
deformations for problems that are innately transient. This leads to hundreds  
of thousands of degrees of freedom, as well as very fine discretizations in time in  
20 order to capture the characteristic times of the problem [3]. Earlier works such  
as the one by Sadeghi and Sui [4] assessed the effects of surface roughness in the  
form of a sinusoidal waviness, a line of work followed by many others [5, 6] and  
more recently by Wang et al [7]. Hooke [8] developed a perturbation analysis of  
the Reynolds equation as a fast analysis to access the global behavior of rough  
25 EHL contacts, under the assumption of small perturbation with respect to the  
smooth case.

Recent efforts have been focused on representing the surface *as it is*, that  
is, inputting the shape of realistic measured surfaces as data in the simulations,  
both for line and point contacts. Morales-Espejel et al [9] presented a fine-scale  
30 EHL model where the evolution of the surface is considered. TEHL contacts  
where both waviness and realistic surfaces are assessed were presented by Wang  
et al [10]. Simulations with measured machined rough surfaces at different  
orientations were carried out by Zhu et al [11], considering transient effects in  
TEHL contacts with a non-Newtonian lubricant. This line of work has also been  
35 followed by [12, 13].

In all of these works the size of the contact region ranges from a few hundred  
micrometers to one millimeter, thus potentially holding hundreds of asperities.  
For other lubricated devices, such as the piston skirt/liner contact the number  
of asperities can rise to the thousands due to the dimensions of the domain,

40 as shown by Zhu et al [14]. Stochastic methods, averaging techniques and flow factors emerged to solve this issue and decouple the microscopic scale from the macroscopic scale, thus reducing the computational cost. From those, the most commonly adopted are Patir and Cheng's [15] flow factors, which are still commonly used in EHL [16, 17, 10].

45 All of these techniques are heuristic solutions to the formal approach which is homogenization. Averaged equations are developed with coefficients being computed in periodic cells (the so-called local problems) with the dimensions of the roughness wavelength. Furthermore, the flow factors can be formally defined, as done by Bayada [18]. The first homogenized results in EHL are due  
50 to Bayada et al [19, 20], where the authors dealt with a Newtonian fluid with piezoviscous effects and density variations. The linearity of the local problems, which is essential for the classic definition of the flow factors, relied on the asymptotic assumption.

Even though the surface roughness wavelength can be smaller in some or-  
55 ders of magnitude compared to the dimensions of the contact, the asymptotic assumption can lead to significant differences compared to the fine-scale solution. As shown by Venner and Lubrecht [21], high frequency roughness is almost undeformed by the fluid pressure, while the large wavelengths are largely affected. In an effort to incorporate the effects of a not-so-small wavelength, some authors  
60 have considered the deformations taking place in the local problems. This is the case of Budt et al [22], who decoupled the microscopic from the macroscopic scale using a FE<sup>2</sup>-type technique. Other authors preferred, in a more heuristic approach, to redefine the Patir and Cheng's flow factors considering the local deformations [23, 24]. A precise definition of the homogenized EHL problem  
65 with finite-wavelength roughness and the corresponding flow factors is given by Scaraggi et al [25, 26]. However, they developed their approach for low contact pressures, and hence the lubricant properties are pressure-independent.

In the present work we propose a homogenized model for the stationary EHL line contact problem that takes into account piezoviscous effects and den-  
70 sity variations with pressure, and where the size of the surface roughness is

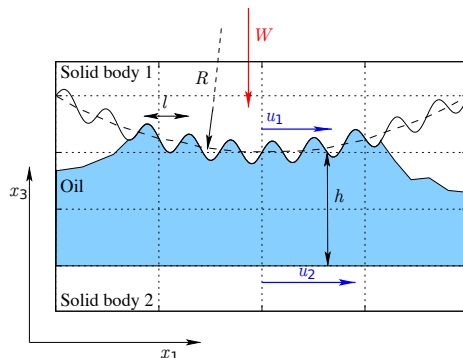


Figure 1: Upper and lower finite solid bodies.

assumed to be non-infinitesimal. Micro-elastohydrodynamic effects were correctly captured in cases of technological interest. Although the developments were made for the one-dimensional stationary case in order to better assess the performance of the model, the extension to the two-dimensional transient case is not burdensome.

The article is outlined as follows: in Section 2 the fine-scale problem is presented in its non-dimensional form. Section 3 deals with generalities of the adopted homogenization technique, the asymptotic homogenized EHL model and the newly developed model. In order to assess the performance of the model herein proposed, a sensitivity analysis is carried out in Section 4. Finally, conclusions are drawn in Section 5.

## 2. Problem statement

We aim to solve stationary lubricated contacts in the elastohydrodynamic (EHL) regime considering piezoviscous effects and density variations with pressure. Cavitation effects are to be taken into account too. The geometry is the one seen in Figure 1: two surfaces separated by a lubricating oil. As we are addressing a stationary problem, surface roughness can be present solely in the fixed surface.

In this work we assume an infinitely long cylinder-on-plane contact. We

assume that the computational domain  $\Gamma^R$  where the fluid dynamics is going to be solved coincides with the  $x_1$  line, Figure 2. We begin by introducing the equation for the gap in the  $x_3$  direction:

$$h(x_1) = h_0 + \frac{x_1^2}{2R} + h_r(x_1) + \delta(x_1) \quad (1)$$

where  $R$  is the reduced radius of curvature in the  $x_1$  direction of the line contact for the mean smooth surface,  $h_0$  parametrizes the translation in the  $x_3$  direction between both solids,  $h_r$  describes the surface roughness (with a zero mean) and  $\delta$  is a function representing the surface deformations due to the elastic behavior of the solids.  $u_1$  and  $u_2$  are respectively the velocities in the  $x_1$  direction of the upper surface (1) and the lower surface (2) with respect to the contact center. We also assume elastic, isotropic, homogeneous solid bodies. The lower body moves in the  $x_1$  direction with prescribed velocity while the upper one is free to move in the  $x_3$  direction only (and thus  $u_1 = 0$ ), its position being parametrized with  $h_0$ . The displacements  $\underline{\delta}(x_1, x_3) = [\delta^{(1)} \ \delta^{(3)}]^T$  induced by the hydrodynamic pressure in the fluid  $p(x_1)$  are given by the elastostatic equation

$$\underline{\text{div}} \underline{\sigma} = \mathbf{0} \quad (2)$$

where  $\underline{\sigma}$  is the Cauchy stress tensor, which is given by Hooke's law

$$\underline{\sigma} = \mathbf{D} \begin{bmatrix} \partial_{x_1} \delta^{(1)} \\ \partial_{x_3} \delta^{(3)} \\ \partial_{x_3} \delta^{(1)} + \partial_{x_1} \delta^{(3)} \end{bmatrix} \quad (3)$$

with

$$\mathbf{D} = \frac{E'}{(1 + \nu')(1 - 2\nu')} \begin{bmatrix} 1 - \nu' & \nu' & 0 \\ \nu' & 1 - \nu' & 0 \\ 0 & 0 & \frac{1 - 2\nu'}{2} \end{bmatrix} \quad (4)$$

$E'$  and  $\nu'$  being the Young's modulus and Poisson's coefficient of the equivalent material, which in terms of the properties of the bodies 1 and 2 are given by

[27]:

$$E' = \frac{E_1^2 E_2 (1 + \nu_2)^2 + E_1 E_2^2 (1 + \nu_1)^2}{(E_1 (1 + \nu_2) + E_2 (1 + \nu_1))^2} \quad (5)$$

$$\nu' = \frac{E_1 \nu_2 (1 + \nu_2) + E_2 \nu_1 (1 + \nu_1)}{E_1 (1 + \nu_2) + E_2 (1 + \nu_1)} \quad (6)$$

From this it can be inferred that the deformations  $\delta$  that affect the gap between the upper and lower solids in equation (1) are

$$\delta(x_1) = \underline{\boldsymbol{\delta}}(x_1, 0) \cdot \underline{\mathbf{e}}_3 = \delta^{(3)}(x_1, 0) \quad (7)$$

where  $\underline{\mathbf{e}}_3$  is the unitary vector in the  $x_3$  direction. Equation (2) is solved in the equivalent domain  $\Omega_s$ , see Figure 2. Notice that the same formulation can be applied even when the lower surface is rough, as we are considering the  
95 equivalent solid. The boundary conditions can be expressed as

- Dirichlet boundary condition:  $\underline{\boldsymbol{\delta}} = \underline{\boldsymbol{\delta}}_D$  on  $\Gamma_D^s$ ,
- von Neumann boundary condition:  $\underline{\boldsymbol{\sigma}} \cdot \underline{\mathbf{n}} = \mathbf{0}$  on  $\Gamma_N^s$ ,
- coupling term with Reynolds equation:  $\underline{\boldsymbol{\sigma}} \cdot \underline{\mathbf{n}} = -p\underline{\mathbf{n}}$  on  $\Gamma^R$ .

where the boundary of the domain  $\partial\Omega_s$  is split into complementary parts  $\partial\Omega_s =$   
100  $\Gamma_D^s \cup \Gamma_N^s \cup \Gamma^R$ . By taking the force exerted by the pressure along  $x_3$  only we disregard the deformations caused by the shear stress in the  $x_1$  direction and we assume small perturbations for the elastic problem. Here  $\underline{\mathbf{n}}$  is the unitary normal to  $\partial\Omega_s$ .

It is assumed also that the thin film approximation is valid, and if we select the frame of reference on the upper surface, then the hydrodynamic pressure  $p(x_1)$  is given by the following form of the Reynolds equation [28]

$$\frac{\partial}{\partial x_1} \left( u_m \rho h - \frac{\rho h^3}{12\mu} \frac{\partial p}{\partial x_1} \right) = 0 \quad (8)$$

Here the density  $\rho = \rho(p)$  and the viscosity  $\mu = \mu(p)$  are functions of the  
105 hydrodynamic pressure, and  $u_m$  is the mean velocity  $u_m = \frac{u_2 + u_1}{2}$ .



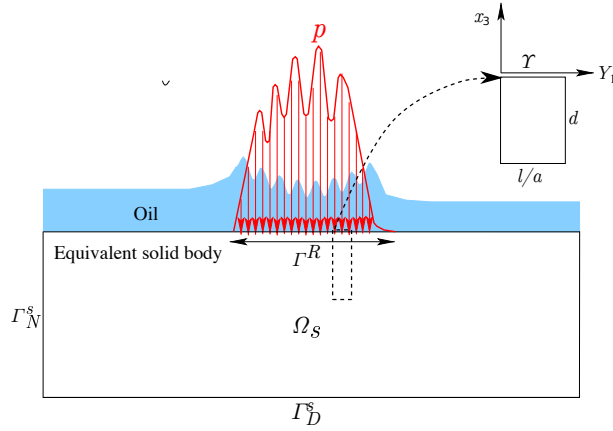


Figure 2: A section of the computational domain.

The load  $W$  applied on the upper solid body must be balanced by the force exerted by the hydrodynamic pressure  $p$ :

$$W = \int_{\Gamma^R} p(x_1) dx_1 \quad (9)$$

Cavitation effects are introduced by means of a penalization method, as in [27]. The penalization method sets a source term  $K_p p^-$  in the Reynolds equation (8), where  $p^- = \min(p, 0)$ , and  $K_p > 0$  is a large penalization constant.

### 2.1. Non-dimensional form

110 We consider the following non-dimensionalizations and definitions:

$$X_1 = \frac{x_1}{a}, \quad X_3 = \frac{x_3}{a}, \quad \underline{\Delta} = \frac{\delta}{a} \quad (10)$$

$$H = \frac{h}{a^2/R}, \quad H_0 = \frac{h_0}{a^2/R}, \quad H_r = \frac{h_r}{a^2/R}, \quad \Delta = \frac{\delta}{a^2/R} \quad (11)$$

$$\bar{u} = \frac{u_m}{u_r}, \quad \bar{\mu} = \frac{\mu}{\mu_r}, \quad \bar{\rho} = \frac{\rho}{\rho_r}, \quad P = \frac{p}{p_h}, \quad \underline{\underline{\Sigma}} = \frac{\underline{\underline{\sigma}}}{p_h} \quad (12)$$

Note that the non-dimensionalization for  $\underline{\Delta}$  and  $\Delta$  are not the same. For a line contact [29] we select  $a$  as the half width of the contact and  $p_h$  as the maximum dry contact pressure of the Hertzian theory:

$$a = \sqrt{\frac{8WR}{\pi E_r}} \quad \text{and} \quad p_h = \frac{2W}{\pi a} \quad (13)$$

with  $\frac{2}{E_r} = \frac{(1-\nu_1^2)}{E_1} + \frac{(1-\nu_2^2)}{E_2}$ . Finally,  $u_r$  is a reference velocity (when  $u_m$  is constant, one can opportunely choose  $u_r = u_m$ ),  $\mu_r$  and  $\rho_r$  are respectively the viscosity and density at atmospheric pressure.

This leads also to the following non-dimensional number:

$$\lambda = \frac{12u_r\mu_r R^2}{a^3 p_h} \quad (14)$$

Then the complete problem to be solved reads:

115 *Problem 1. Fine-scale reference problem.* Given the constants (boundary conditions, geometry, material)  $P_D$ ,  $\underline{\Delta}_D$ ,  $\bar{u}$ ,  $\lambda$ ,  $K_p$ ,  $E'/p_h$  and  $\nu'$ , the known functions  $H_r(X_1)$ ,  $\bar{\rho}(P)$  and  $\bar{\mu}(P)$ , find  $H_0$ ,  $P(X_1)$  and  $\underline{\Delta}(X_1, X_3)$  satisfying:

- Reynolds equation:

$$\frac{\partial}{\partial X_1} \left( \bar{u} \bar{\rho} H - \epsilon \frac{\partial P}{\partial X_1} \right) + K_p P^- = 0 \quad (15)$$

where  $\epsilon = \frac{\bar{\rho} H^3}{\bar{\mu} \lambda}$ ,  $P^- = \min(P, 0)$  and  $H(X_1) = H_0 + \frac{X_1^2}{2} + H_r(X_1) + \Delta(X_1)$ , and with the boundary conditions:  $P(X_1) = P_D$  on  $\Gamma^R$ .

- Load balance:

$$\int_{\Gamma^R} P dX_1 = \frac{\pi}{2} \quad (16)$$

- Elastostatic problem:

$$\Delta(X_1) = \frac{R}{a} \underline{\Delta}(X_1, 0) \cdot \underline{\mathbf{e}}_3 \text{ on } \Gamma^R \quad (17)$$

where  $\underline{\Delta} = (\Delta^{(1)}, \Delta^{(3)})$  is the solution of

$$\underline{\text{div}} \underline{\underline{\Sigma}} = \mathbf{0} \quad (18)$$

with  $\underline{\underline{\Sigma}}$  the Cauchy stress tensor

$$\underline{\underline{\Sigma}} = \frac{1}{p_h} \mathbf{D} \begin{bmatrix} \partial_{X_1} \Delta^{(1)} \\ \partial_{X_3} \Delta^{(3)} \\ \partial_{X_3} \Delta^{(1)} + \partial_{X_1} \Delta^{(3)} \end{bmatrix} \quad (19)$$

and boundary conditions  $\underline{\Delta} = \underline{\Delta}_D$  on  $\Gamma_D^s$ ,  $\underline{\underline{\Sigma}} \cdot \underline{\mathbf{n}} = \mathbf{0}$  on  $\Gamma_N^s$  and

$$\underline{\underline{\Sigma}} \cdot \underline{\mathbf{n}} = -P \underline{\mathbf{n}} \text{ on } \Gamma^R \quad (20)$$

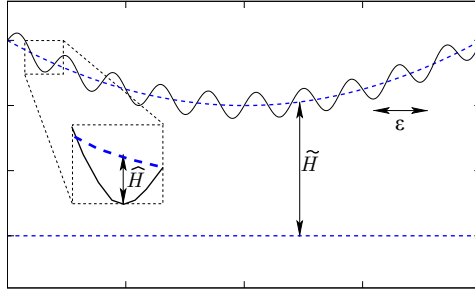


Figure 3: Separating the macroscopic scale from the microscopic scale.

120 *2.2. Separation of scales*

Assuming a periodic roughness of dimensional spatial period  $l$ , Figure 3 illustrates that the surface is composed of a slow-varying part (dashed line) and a fast varying part (full line). With this in mind, the equation for the gap (1) can be rewritten as

$$H(X_1) = \tilde{H}(X_1) + \hat{H}(X_1) \quad (21)$$

where  $\tilde{H}(X_1)$  represents the smooth, larger scale of the gap  $H$

$$\tilde{H}(X_1) = H_0 + \frac{X_1^2}{2} + \tilde{\Delta}(X_1) \quad (22)$$

and  $\hat{H}(X_1)$  the smaller scale, with periodicity  $\varepsilon = l/a$  which is the non-dimensional wavelength of the roughness.  $\varepsilon$  is also the scale ratio, expected to be small, between the roughness and the overall contact. Then  $\hat{H}$  can be expressed as

$$\hat{H}(X_1) = H_r \left( \frac{X_1}{\varepsilon} - \xi \right) + \hat{\Delta} \left( X_1, \frac{X_1}{\varepsilon} - \xi \right) \quad (23)$$

Here  $H_r$  represents the undeformed shape of the roughness, which we assume is periodic in  $\varepsilon$ , and  $\xi$  is a phase shift. Both  $\tilde{\Delta}$  and  $\hat{\Delta}$  represent solid deformations in the large and small scale respectively, although their precise definition is postponed.

125 **3. Homogenization of the elastohydrodynamic lubrication problem**

The periodic roughness introduces a new variable

$$Y_1 = \frac{X_1}{\varepsilon} - \xi \quad (24)$$

which we can define in a non-dimensional domain  $\Upsilon = [0, 1]$  (see Figure 2).

Then, the expression for the gap between the lubricated surfaces becomes

$$H(X_1, Y_1) = \tilde{H}(X_1) + \hat{H}(X_1, Y_1) \quad (25)$$

In the method of asymptotic expansions it is assumed that the hydrodynamic pressure can be expanded as:

$$P = P(X_1, Y_1) = P_0(X_1, Y_1) + \varepsilon P_1(X_1, Y_1) + \varepsilon^2 P_2(X_1, Y_1) + \dots \quad (26)$$

where  $P_0, P_1, \dots$  are periodic in  $Y_1$ , and following (24) the derivative with respect to  $X_1$  is replaced with

$$\frac{\partial}{\partial X_1} + \frac{1}{\varepsilon} \frac{\partial}{\partial Y_1} \quad (27)$$

As the term  $P^-$  of the penalization method is not smooth, it cannot be expanded easily; the cavitation condition will be treated separately and is not considered at this point. Introducing (26) and (27) into equation (15) and considering the leading terms in the resulting expansion, that is, the terms in  $\varepsilon^{-2}$ ,  $\varepsilon^{-1}$  and  $\varepsilon^0$  respectively we have

$$\frac{\partial}{\partial Y_1} \left( \epsilon \frac{\partial P_0}{\partial Y_1} \right) = 0 \quad (28)$$

$$\frac{\partial}{\partial Y_1} (\bar{\rho} \bar{u} H) - \frac{\partial}{\partial X_1} \left( \epsilon \frac{\partial P_0}{\partial Y_1} \right) - \frac{\partial}{\partial Y_1} \left( \epsilon \frac{\partial P_0}{\partial X_1} \right) - \frac{\partial}{\partial Y_1} \left( \epsilon \frac{\partial P_1}{\partial Y_1} \right) = 0 \quad (29)$$

$$\frac{\partial}{\partial X_1} (\bar{\rho} \bar{u} H) - \frac{\partial}{\partial X_1} \left( \epsilon \frac{\partial P_0}{\partial X_1} \right) - \frac{\partial}{\partial X_1} \left( \epsilon \frac{\partial P_1}{\partial Y_1} \right) - \frac{\partial}{\partial Y_1} \left( \epsilon \frac{\partial P_1}{\partial X_1} \right) - \frac{\partial}{\partial Y_1} \left( \epsilon \frac{\partial P_2}{\partial Y_1} \right) = 0 \quad (30)$$

and in the solid body, we have through the boundary conditions

$$\underline{\underline{\Sigma}} \cdot \mathbf{n} = -(P_0 + \varepsilon P_1 + \dots) \mathbf{n} \text{ on } \Gamma^R \quad (31)$$

The linearity in this last equation and in the solid deformations problem allows us to expand the displacements  $\underline{\underline{\Delta}}$  into

$$\underline{\underline{\Delta}} = \underline{\underline{\Delta}}(X_1, Y_1) = \underline{\underline{\Delta}}_0(X_1, Y_1) + \varepsilon \underline{\underline{\Delta}}_1(X_1, Y_1) + \varepsilon^2 \underline{\underline{\Delta}}_2(X_1, Y_1) + \dots \quad (32)$$

where each  $\underline{\Delta}_i$  is due to  $P_i$ ,  $i = 0, 1, 2, \dots$  respectively, by expanding the linear elastic problem with respect to  $\varepsilon$ , and is  $Y_1$ -periodic. These developments allows the problem to be split as described in the following sections.

The load balance equation (16) is also expanded, leading to:

$$\int_{\Gamma^R} P_0 dX_1 = \frac{\pi}{2} \quad (33)$$

$$\langle P_1 \rangle = 0 \quad (34)$$

where  $\langle \cdot \rangle$  denotes the average over the  $\Upsilon$  domain.

### 3.1. The classical homogenized asymptotic (H-A) model

These classical results in asymptotic homogenization on the EHL problem are due to Bayada et al [19] and are briefly recalled here. If we assume an infinitesimal  $\varepsilon$ , and also that the terms in  $\varepsilon, \varepsilon^2, \dots$  in equation (26) are negligible with respect to  $P_0$ , then expanding  $H, \bar{\rho}$  and  $\varepsilon$ , it can be proven that equations (28) to (30) become

$$\frac{\partial}{\partial Y_1} \left( \epsilon_0 \frac{\partial P_0}{\partial Y_1} \right) = 0 \quad (35)$$

$$\frac{\partial}{\partial Y_1} (\bar{\rho}_0 \bar{u} H) - \frac{\partial}{\partial X_1} \left( \epsilon_0 \frac{\partial P_0}{\partial Y_1} \right) - \frac{\partial}{\partial Y_1} \left( \epsilon_0 \frac{\partial P_0}{\partial X_1} \right) - \frac{\partial}{\partial Y_1} \left( \epsilon_0 \frac{\partial P_1}{\partial Y_1} \right) = 0 \quad (36)$$

$$\frac{\partial}{\partial X_1} (\bar{\rho}_0 \bar{u} H) - \frac{\partial}{\partial X_1} \left( \epsilon_0 \frac{\partial P_0}{\partial X_1} \right) - \frac{\partial}{\partial X_1} \left( \epsilon_0 \frac{\partial P_1}{\partial Y_1} \right) - \frac{\partial}{\partial Y_1} \left( \epsilon_0 \frac{\partial P_1}{\partial X_1} \right) - \frac{\partial}{\partial Y_1} \left( \epsilon_0 \frac{\partial P_2}{\partial Y_1} \right) = 0 \quad (37)$$

with

$$\bar{\rho}_0 = \bar{\rho}(P_0), \bar{\mu}_0 = \bar{\mu}(P_0), \epsilon_0 = \frac{\bar{\rho}_0 H^3}{\bar{\mu}_0 \lambda} \quad (38)$$

$$H = \tilde{H} + H_r, \tilde{H} = H_0 + \frac{X_1^2}{2} + \Delta_0 \quad (39)$$

#### 3.1.1. Microscopic problem

From equation (35) it can be inferred that  $P_0 = P_0(X_1)$ , and thus  $\tilde{\Delta} = \Delta_0(X_1)$  are macroscopic displacements computed on  $\Omega_s$ . Notice that there are only macroscopic deformations in the expression for the clearance  $H$  (39), i.e.  $\hat{\Delta} = 0$ . Taking this into account, equation (36) becomes linear on  $P_1$ :

$$\frac{\partial}{\partial Y_1} (\bar{\rho}_0 \bar{u} H) - \frac{\partial}{\partial Y_1} \left( \epsilon_0 \frac{\partial P_0}{\partial X_1} \right) - \frac{\partial}{\partial Y_1} \left( \epsilon_0 \frac{\partial P_1}{\partial Y_1} \right) = 0 \quad (40)$$

This problem for the microscopic pressure  $P_1$  is determined up to a constant  
of  $X_1$ . This constant is fixed using the micro load balance equation (34).

### 3.1.2. Macroscopic problem

Averaging (37) leads to:

$$\frac{\partial}{\partial X_1} (\overline{\rho_0 u} \langle H \rangle) - \frac{\partial}{\partial X_1} \left( \langle \epsilon_0 \rangle \frac{\partial P_0}{\partial X_1} \right) - \frac{\partial}{\partial X_1} \left( \langle \epsilon_0 \rangle \frac{\partial P_1}{\partial Y_1} \right) = 0 \quad (41)$$

This is the equation for the macroscopic pressure  $P_0$ . Since  $H_0$  is also an unknown in the expression of the film thickness  $H$ , an additional equation to close the problem is the macro load balance (33).

As mentioned previously, the elastostatic problem is only derived at macroscale:  $\Delta_0(X_1) = \frac{R}{a} \underline{\Delta}_0(X_1, 0) \cdot \underline{e}_3$  on  $\Gamma^R$ , where  $\underline{\Delta}_0 = (\Delta_0^{(1)}, \Delta_0^{(3)})$  is the solution of

$$\underline{\text{div}} \underline{\underline{\Sigma}}_0 = \mathbf{0} \quad (42)$$

with

$$\underline{\underline{\Sigma}}_0 = \frac{1}{p_h} \mathbf{D} \begin{bmatrix} \partial_{X_1} \Delta_0^{(1)} \\ \partial_{X_3} \Delta_0^{(3)} \\ \partial_{X_3} \Delta_0^{(1)} + \partial_{X_1} \Delta_0^{(3)} \end{bmatrix} \quad (43)$$

and boundary conditions  $\underline{\Delta}_0 = \underline{\Delta}_D$  on  $\Gamma_D^s$ ,  $\underline{\underline{\Sigma}}_0 \cdot \underline{n} = \mathbf{0}$  on  $\Gamma_N^s$  and

$$\underline{\underline{\Sigma}}_0 \cdot \underline{n} = -P_0 \underline{n} \text{ on } \Gamma^R \quad (44)$$

### 3.1.3. Relocalization

Although the homogenized asymptotic model is developed for a infinitesimal  $\varepsilon$ , it is still expected that it can approximate the solution of the reference problem with a finite wavelength  $\varepsilon_0$  in certain situations, such as when  $\varepsilon_0$  and roughness amplitude are small enough. Thus, the hydrodynamic pressure can be reconstructed as

$$P(X_1) \simeq P_0(X_1) + \varepsilon_0 P_1(X_1, Y_1) = P_0(X_1) + \varepsilon_0 P_1(X_1, X_1 - \varepsilon_0 \left\lfloor \frac{X_1}{\varepsilon_0} \right\rfloor - \xi) \quad (45)$$

where  $\lfloor \cdot \rfloor$  is the floor function, returning the greatest integer less or equal than  $(\cdot)$ .

### 3.2. The homogenized $\mu$ -EHL model

The classical asymptotic homogenization does not involve piezoviscous effects nor elasticity at the microscopic scale. It is only valid if  $\varepsilon_0 P_1$  is very small when compared to  $P_0$ . This constitutes a limitation of this approach, leading to inaccurate solutions for severe loading conditions, i.e., when the film thickness is not very large when compared to the roughness amplitude. The homogenized  $\mu$ -EHL model is intended to overcome these limitations. We assume the same expansion of equation (26), however, we will not develop the constitutive laws  $\bar{\rho}$ ,  $\bar{\mu}$  and the coefficient  $\epsilon$  in equations (28) to (30). For those terms, we will consider the finite roughness wavelength  $\varepsilon_0$  such that

$$\bar{\rho} = \bar{\rho}(P_0 + \varepsilon_0 P_1), \bar{\mu} = \bar{\mu}(P_0 + \varepsilon_0 P_1), \epsilon = \frac{\bar{\rho} H^3}{\bar{\mu} \lambda} \quad (46)$$

and

$$H = \tilde{H} + \hat{H}, \tilde{H} = H_0 + \frac{X_1^2}{2} + \Delta_0, \hat{H} = H_r + \varepsilon_0 \Delta_1 \quad (47)$$

with  $\Delta_1$  being microscopic displacements to be fully defined in the following sections. Here the higher order terms in  $\varepsilon_0^2, \varepsilon_0^3, \dots$ , are still neglected.

#### 3.2.1. Microscopic problem

As in the classical asymptotic model, from equation (35) it can be deduced again that  $P_0 = P_0(X_1)$  and thus  $\underline{\Delta}_0 = \underline{\Delta}_0(X_1)$  too. The microscopic problems for the pressure are now the non-linear equation in  $P_1$

$$\frac{\partial}{\partial Y_1} (\bar{\rho} \bar{u} H) - \frac{\partial}{\partial Y_1} \left( \epsilon \frac{\partial P_0}{\partial X_1} \right) - \frac{\partial}{\partial Y_1} \left( \epsilon \frac{\partial P_1}{\partial Y_1} \right) = 0 \quad (48)$$

Again, the problem is determined up to a constant of  $X_1$ , however, contrary to the homogenized asymptotic model this constant affects also the solution of the macro pressure  $P_0$ , as can be seen from the dependency of  $\bar{\mu}$  and  $\bar{\rho}$  with  $P_1$ .

The assumption of a non-negligible  $\varepsilon_0 P_1$  term leads to non-negligible displacements  $\varepsilon_0 \Delta_1$ . An elastic problem (yet to be defined) must be solved, with a boundary condition with pressure  $P_1$  on  $\Upsilon \times \{0\}$ . Notice that  $P_1 = P_1(X_1, Y_1)$  introduces the fast variable  $Y_1$  in the elastic deformations problem.

Due to the zero average of  $P_1$  over  $\Upsilon$ , Saint Venant's principle implies that  
155 the deformations induced by this force will be localized, i.e., they won't prop-  
agate far away from the area of application of  $P_1$ . This assumption allows us  
to solve these micro-deformations in a reduced domain  $\Upsilon \times [0, d]$  (see Figure  
2), where the length  $d$  is determined by the roughness wavelength  $\varepsilon_0$  and the  
equivalent Poisson's coefficient  $\nu'$  (assuming  $\nu'$  not close to 0.5 for which Saint  
160 Venant's principle is not valid).

This new problem in  $\Upsilon \times [0, d]$  (see Figure 2) is in the variables  $Y_1$  and  
 $Y_3 = X_3/\varepsilon_0$ . Notice that at each point  $X_1$  an independent problem has to be  
solved in  $\Upsilon \times [0, d]$ , which is parametrized by  $P_0$ ,  $\tilde{H}$  and  $\partial_{X_1} P_0$  in contrast  
with the microscopic problems of the classical model, which only depend on  
two parameters,  $\tilde{H}$  and  $\partial_{X_1} P_0$ . Then the equation for the elastic deformations  
 $\underline{\Delta}_1(X_1, Y_1, Y_3) = (\Delta_1^{(1)}, \Delta_1^{(3)})$  is

$$\underline{\text{div}}_Y \underline{\underline{\Sigma}}_1 = 0 \quad (49)$$

where  $\underline{\text{div}}_Y$  is the divergence operator with respect to the coordinates  $(Y_1, Y_3)$ ,  
and  $\underline{\underline{\Sigma}}_1$  is the micro Cauchy stress tensor in the solid  $\Upsilon \times [0, d]$ :

$$\underline{\underline{\Sigma}}_1 = \frac{1}{p_h} \mathbf{D} \begin{bmatrix} \partial_{Y_1} \Delta_1^{(1)} \\ \partial_{Y_3} \Delta_1^{(3)} \\ \partial_{Y_3} \Delta_1^{(1)} + \partial_{Y_1} \Delta_1^{(3)} \end{bmatrix} \quad (50)$$

In  $\{0\} \times [0, d]$  and  $\{\varepsilon_0\} \times [0, d]$  the only requirement that we have is periodicity  
of  $\underline{\Delta}_1$  in the  $Y_1$  variable:

$$\underline{\Delta}_1(X_1, 0, Y_3) = \underline{\Delta}_1(X_1, \varepsilon_0, Y_3) \quad (51)$$

We assume that  $\Upsilon \times \{d\}$  is sufficiently far away from the localized deforma-  
tions at  $\Upsilon \times \{0\}$ , so that we can set the Dirichlet boundary conditions:

$$\underline{\Delta}_1 = \underline{\underline{C}} \text{ on } Y \times \{d\} \quad (52)$$

where  $\underline{\underline{C}}$  is a constant to be determined with  $\langle \Delta_1 \rangle = 0$ , and the boundary  
condition coupling the micro-elastostatics to the micro Reynolds equation:

$$\underline{\underline{\Sigma}}_1 \cdot \underline{\mathbf{n}} = -P_1 \underline{\mathbf{n}} \text{ on } \Gamma^R \quad (53)$$



Particularly, we are interested at the deformations at the surface  $\Upsilon \times \{0\}$

$$\Delta_1(X_1, Y_1) = \varepsilon_0 \frac{R}{a} \underline{\Delta}_1(X_1, Y_1, 0) \cdot \underline{\mathbf{e}}_3 \quad (54)$$

where the factor  $\varepsilon_0$  stands from the difference between the scaling factors of the elastic problem and the gap  $H$  in the microscopic Reynolds equation in  $\underline{\mathbf{e}}_3$  direction.

### 3.2.2. Macroscopic problem

Taking the average of equation (37) we now obtain:

$$\frac{\partial}{\partial X_1} (\bar{u} \langle \bar{\rho} H \rangle) - \frac{\partial}{\partial X_1} \left( \langle \epsilon \frac{\partial P_0}{\partial X_1} \rangle \right) - \frac{\partial}{\partial X_1} \left( \langle \epsilon \frac{\partial P_1}{\partial Y_1} \rangle \right) = 0 \quad (55)$$

We assume the pressure boundary conditions  $P_D$  to be only a function of the slow variable  $X_1$ , so it reads

$$P_0(X_1) = P_D \text{ on } \partial\Gamma^R \quad (56)$$

165 The macroscale displacements  $\Delta_0$  come from the solution of the elastostatic equation with  $P_0$  as von Neumann boundary conditions, as in the classical asymptotic model.

### 3.2.3. Dealing with cavitation in the two-scale model

For the homogenized models we propose to introduce penalization terms in both the microscale and the macroscale equations, taking into account that the condition for cavitation  $P_0 + \varepsilon_0 P_1 \geq 0$  can be traduced into a restriction for the microscopic pressure

$$P_1 \geq -\frac{P_0}{\varepsilon_0} \quad (57)$$

However, imposing the cavitation condition only in the microscopic pressure is not feasible. A physical argument against it is that the large negative pressures arising in the divergent part of the lubricated contact could not be suppressed by the small pressures developed in small or even moderately small roughness. Hence, constraints will be set both on the macroscopic and microscopic pressures. Then, the penalization term for the macroscopic equation is

$K_p P_0^-$  with

$$P_0^- = \min(P_0, 0) \quad (58)$$

and the one for the microscopic equation is  $K_p P_1^-$ , with  $P_1^-$  defined with

$$P_1^- = \min\left(P_1 + \frac{P_0}{\varepsilon_0}, 0\right) \quad (59)$$

while it is not necessary that the constant  $K_p$  be the same for both penalization  
 170 terms. It should be noticed that the penalization method allows small negative  
 pressures to take place. If  $P_0 \leq 0$  at a certain point in the domain, the condition  
 set by the equation (57) will lead to an incompatibility with  $\langle P_1 \rangle = 0$ . In order  
 to avoid this we will set  $P_1 \equiv 0$  at all the points  $X_1$  of the macroscopic domain  
 where  $P_0 \leq 0$ . This is consistent with the straight application of cavitation  
 175 unilateral constraint: indeed when a macro cavitation takes place (i.e.  $P_0 = 0$ )  
 the constraint  $\langle P_1 \rangle = 0$  together with  $P_1 \geq -\frac{P_0}{\varepsilon_0} = 0$  leads also to  $P_1 = 0$ .

Thus, we can summarize the  $\mu$ -EHL model as:

*Problem 2. Homogenized  $\mu$ -EHL problem.* Given the constants (boundary con-  
 ditions, geometry, material)  $P_D$ ,  $\underline{\Delta}_D$ ,  $\bar{u}$ ,  $\varepsilon_0$ ,  $\lambda$ ,  $K_p$ ,  $E'/P_h$  and  $\nu'$ , the known  
 180 functions  $H_r(Y_1)$ ,  $\bar{\rho}(P_0 + \varepsilon_0 P_1)$  and  $\bar{\mu}(P_0 + \varepsilon_0 P_1)$ , find the macroscopic quanti-  
 ties  $H_0$ ,  $P_0(X_1)$ ,  $\Delta_0(X_1)$  and the microscopic corrections  $P_1(X_1, Y_1)$ ,  $\Delta_1(X_1, Y_1)$   
 (with  $\langle P_1 \rangle = \langle \Delta_1 \rangle = 0$  and  $Y_1$ -periodicity) satisfying:

- the two-scale Reynolds equations with  $\epsilon = \frac{\bar{\rho} H^3}{\bar{\mu} \lambda}$ :

$$\frac{\partial}{\partial X_1} (\bar{u} \langle \bar{\rho} H \rangle) - \frac{\partial}{\partial X_1} \left( \langle \epsilon \rangle \frac{\partial P_0}{\partial X_1} \right) - \frac{\partial}{\partial X_1} \left( \langle \epsilon \frac{\partial P_1}{\partial Y_1} \rangle \right) + K_p P_0^- = 0 \quad (60)$$

$$\frac{\partial}{\partial Y_1} (\bar{\rho} \bar{u} H) - \frac{\partial}{\partial Y_1} \left( \epsilon \frac{\partial P_0}{\partial X_1} \right) - \frac{\partial}{\partial Y_1} \left( \epsilon \frac{\partial P_1}{\partial Y_1} \right) + K_p P_1^- = 0 \quad (61)$$

this last one being superseded by  $P_1(X_1, Y_1) \equiv 0$  if  $P_0(X_1) \leq 0$ , and the  
 film thickness  $H$  being (47).

- 185 • the load balance equation (33)
- the two-scale elastostatic problem (42, 43, 44) and (49, 50, 53)

#### 4. Validation of the homogenized $\mu$ -EHL model

Let us first outline the fine-scale reference problem. The non-dimensional computational domain for the Reynolds equation is defined in  $\Gamma^R = [-4, 2]$ ; the elastic body is defined on  $\Omega_s = [-35, 25] \times [-60, 0]$ , see Figure 4.

The boundary conditions are set as  $P_D = 0$ ,  $\underline{\Delta}_D = 0$ ; the velocity is set to  $\bar{u} = 1$ .

The non-dimensional expression for the laws governing the compressibility of the fluid and the piezoviscosity chosen for the numerical tests are

$$\bar{\rho} = 1 + \frac{c_A p}{1 + c_B p} \quad (62)$$

$$\bar{\mu} = \left( \frac{\mu_\infty}{\mu_r} \right)^{1 - (1 + \frac{p}{\gamma})^c} \quad (63)$$

the first one being a proposal of Dowson and Higginson [30] and the former by Roelands [31], where  $\mu_\infty = 6.31 \times 10^{-5}$  Pa.s and  $\gamma = 1.961 \times 10^8$  Pa are constants of the model. Here we have chosen  $c_A = 6 \times 10^{-10}$  Pa $^{-1}$ ,  $c_B = 2 \times 10^{-9}$  Pa $^{-1}$ ,  $\mu_r = 0.004$  Pa.s, and  $c = 0.5$ .

The non-dimensional penalty method constant here taken is  $K_p = 1000$  for every simulation.

On the upper surface we set sinusoidal periodic textures, given by the equation:

$$H_r(X_1) = A \sin \left( 2\pi \left( \frac{X_1}{\varepsilon_0} - \xi \right) \right) = A \sin(2\pi Y_1) = H_r(Y_1) \quad (64)$$

where  $A$  is the non-dimensional roughness amplitude.

In order to define a maximum value for the amplitude  $A$  of the roughness in the simulations, we will use the film thickness ratio

$$\Lambda = \frac{H_{\min}}{\sigma} \quad (65)$$

where  $\sigma$  is the root mean square value of the non-dimensional combined roughness of both surfaces in contact, and thus here equal to  $\sigma = \frac{\sqrt{2}}{2} A$ . The minimum film thickness is  $H_{\min} = \min_{\Gamma^R} H$ .

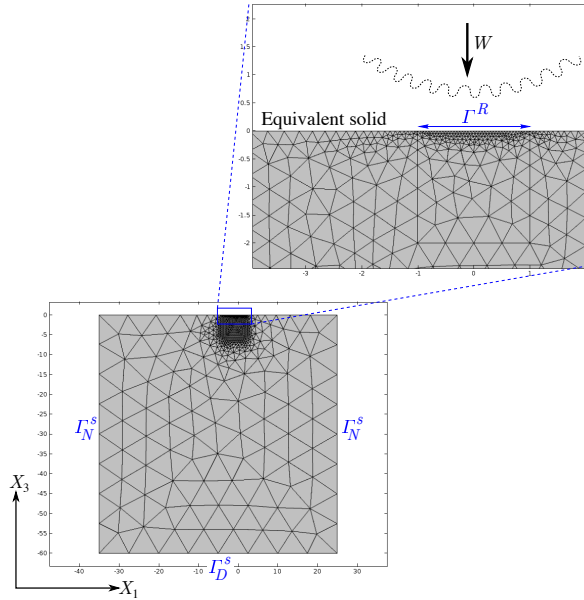


Figure 4: A finite element mesh on the equivalent solid (domain  $\Omega_s$ ) and on the domain where the Reynolds equation is solved ( $\Gamma^R$ ).

For elastohydrodynamic lubrication some authors [28, 32] suggest  $3 < \Lambda < 10$ . Here we will take a minimum film thickness ratio of  $\Lambda = 5.66$ , which gives us  $A = 0.25H_{\min}$ . As  $H_{\min}$  is not known a priori, then the maximum  $A$  will be taken as a fraction of  $H_{\min, A=0}$ , that is, the minimum film thickness of the smooth problem (no surface roughness):

$$A_{\text{rel}} = \frac{A}{H_{\min, A=0}} \quad (66)$$

To assess the differences between the reference, the homogenized asymptotic and the homogenized  $\mu$ -EHL models, several values of the roughness wavelength  $\varepsilon_0$  and amplitude  $A$  will be explored.

What remains to define the problem are three non-dimensional quantities:  $\lambda$ ,  $E'/p_h$  and  $\nu'$ . The  $\lambda$  parameter is a measure of the relevance of the fluid dynamics effects compared to the solid deformations, while  $E'/p_h$  gives us a measure of the importance of the solid deformations. A larger  $E'/p_h$  means a stiffer solid or a lower load imposed on the lubricated contact. In every numerical

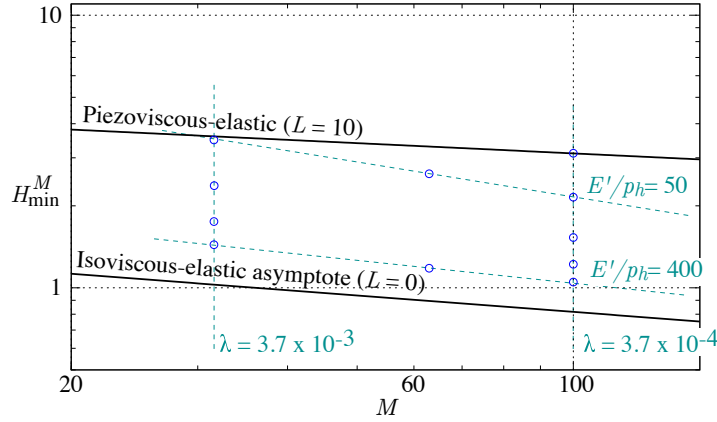


Figure 5: Numerical tests were carried out for the  $M$ ,  $L$  ( $\lambda$ ,  $E'/p_h$ ) values marked by the blue circles. The dashed lines represent configurations of constant  $E'/p_h$  and  $\lambda$ . At each point several roughness configurations ( $A_{\text{rel}}$ ,  $\varepsilon_0$ ,  $\xi$ ) were assessed.

test we will adopt a fixed value of  $\nu' = 0.3$ , while the other two parameters will take values corresponding to cases of technological interest. This choice is based on the fact that the Poisson ratio of typical metallic materials is around 0.3 and that the solution will not vary significantly for those values. In order to put the results into the perspective of the tribology community, along with the  $\lambda$ ,  $E'/p_h$  and  $\nu'$  parameters that define each problem we will provide the Moes-Venner parameters [33]

$$M = \frac{W}{\sqrt{2u_m E_r R \mu_r}}, \quad L = \alpha E_r^{3/4} \left( \frac{2u_m \mu_r}{R} \right)^{1/4} \quad (67)$$

with  $\alpha = c \ln(\mu_r/\mu_\infty)/\gamma$  being the pressure-viscosity coefficient. Figure 5 shows the Moes parameters for which simulations were ran, with

$$H_m^M = \frac{H_{\min}}{a^2/R} \sqrt{\frac{E_r}{2u_m \mu_r R}} \quad (68)$$

At each point a substantial number of roughness configurations were appraised.

To illustrate this in a more tangible manner, these values are consistent with the parameters of Table 1.

The Reynolds and the elastostatic equations were discretized by means of the  
 210 finite element method, with second order Lagrange elements. The microscopic

$M$	$L$	$\lambda$	$E'/p_h$	$p_h$ /GPa	$a$ /m	$R$ /m	$u_r$ /(m/s)
100	0.66	$3.7 \times 10^{-4}$	400	0.25	0.025	5.51	1
100	1.33	$3.7 \times 10^{-4}$	200	0.50	0.031	0.34	1
100	2.65	$3.7 \times 10^{-4}$	100	1.00	$3.9 \times 10^{-3}$	0.022	1
100	5.30	$3.7 \times 10^{-4}$	50	2.00	$4.9 \times 10^{-5}$	$1.3 \times 10^{-3}$	1
31.6	1.18	$3.7 \times 10^{-3}$	400	0.25	0.025	5.51	10
31.6	2.36	$3.7 \times 10^{-3}$	200	0.50	$3.1 \times 10^{-3}$	0.34	10
31.6	4.72	$3.7 \times 10^{-3}$	100	1.00	$3.9 \times 10^{-4}$	0.022	10
31.6	9.43	$3.7 \times 10^{-3}$	50	2.00	$4.9 \times 10^{-5}$	$1.3 \times 10^{-3}$	10
63.3	0.83	$9.3 \times 10^{-4}$	400	0.25	0.025	5.51	2.5
63.3	6.67	$9.3 \times 10^{-4}$	50	2.00	$4.9 \times 10^{-5}$	$1.3 \times 10^{-3}$	2.5

Table 1: Parameters corresponding to the cases depicted in Figure 5.

problems of the homogenized models were solved at each node of the mesh of the macroscopic problem in a FE<sup>2</sup>-homogenization manner (such as in [34]). This leads to a large number of degrees of freedom, however, as we aim to assess the accuracy of the model here proposed we want to eliminate sources of error, e.g. the ones coming from the decoupling of the macro-scale equations from the microscopic equations. Nonetheless, this will restrict our capacity to solve problems for small  $\varepsilon_0$  values.

A monolithic Newton-Raphson solver is used for the non-linear systems and all linear system of equations are solved using direct methods. Results were computed using commercial software (COMSOL Multiphysics<sup>R</sup> version 5.2a).

Due to the lack of existence of known analytical solutions, all simulated cases will be compared against the reference solution computed in a very fine mesh where the  $[-1, 1]$  region of  $\Gamma^R$  is discretized into finite elements of size  $\Delta X_1 = 1 \times 10^{-4}$ . This discretization leads to 743 134 degrees of freedom in the reference problem and negligible differences in the solution with respect to even finer meshes. For the homogenized models, the  $[-1, 1]$  region of  $\Gamma^R$  of the macro-

scale equations was discretized with finite elements of the size of the roughness wavelength:  $\Delta X_1 = \varepsilon_0$ , and enough finite elements in the micro-problems to ensure mesh convergence. The error computed for a certain field  $Q$  is

$$e_Q = \frac{\|Q - Q_{\text{ref}}\|_{L^2(\Omega)}}{\|Q_{\text{ref}}\|_{L^2(\Omega)}} \quad (69)$$

where  $Q_{\text{ref}}$  is the mesh-converged fine-scale solution and the norms are  $L^2$ -norms taken in the corresponding domain  $\Omega$ .

#### 4.1. Scope of the homogenized asymptotic (H-A) and homogenized $\mu$ -EHL models

225 If the roughness wavelength  $\varepsilon_0$  and amplitude  $A_{\text{rel}}$  are small enough, then the classical homogenized asymptotic and the  $\mu$ -EHL give similar models; in particular they are expected to be accurate approximations of the reference problem. We are interested in the more realistic case of a small but not infinitesimal roughness wavelength  $\varepsilon_0$  nor amplitude  $A_{\text{rel}}$ . To assess the model  
230 ranges of validity, we start at a low  $L$  value of 0.66 and  $M = 100$ . Errors in pressure  $e_P$  are presented for several  $\varepsilon_0$  and  $A_{\text{rel}}$  pairs on Table 2.

As can be seen in Table 2, the errors for the classical homogenized asymptotic model (H-A) grow rapidly with both variables. Figures 6-(b) for  $\varepsilon_0 = 0.05$  and 6-(d) show how the model disregards the microscopic deformations at the  
235 asperity level, which leads to microscopic pressures larger than the ones of the reference solution. In behalf of this, the micro-pressures grow with  $\varepsilon_0$ , as shown in Figures 6-(a) and 6-(c), which correspond to errors of 12.1% and 55.1% respectively. This explains the trends displayed in Table 2. Larger values of  $L$  induce even larger errors, which leads to the conclusion that the classical ho-  
240 mogenized asymptotic model will return satisfactory results only for very low  $L$  values. This shows its inadequacy to approximate the reference solution when  $\varepsilon_0$  is not infinitesimal. On the other hand, the errors attained with the  $\mu$ -EHL model are low, and in every computed case in Table 2 they are below 0.5%. They tend to grow slightly with the roughness amplitude, however, due to the

(a) H-A				
-----				
$A_{\text{rel}}$				
-----				
	0.05	0.15	0.25	
-----				
	0.05	2.67	7.75	12.1
$\varepsilon_0$	0.1	6.13	17.7	27.3
	0.2	13.4	35.7	55.1
-----				

(b) $\mu$ -EHL				
-----				
$A_{\text{rel}}$				
-----				
	0.05	0.15	0.25	
-----				
	0.05	0.12	0.21	0.37
$\varepsilon_0$	0.1	0.11	0.23	0.29
	0.2	0.11	0.22	0.30
-----				

Table 2: Percentage errors in pressure  $e_P$ , relative to the reference solution for  $E'/p_h = 400$  and  $\lambda = 3.7 \times 10^{-4}$  for several roughness wavelengths  $\varepsilon_0$  and amplitudes  $A_{\text{rel}}$ . These cases correspond to Moes parameters of  $M = 100$  and  $L = 0.66$ .

245 low errors with differences in the tenths of percent a clear trend is not perceived  
while varying  $\varepsilon_0$ .

#### 4.2. A sensitivity study

The accuracy of the homogenized  $\mu$ -EHL approximation is here analyzed. As discussed in the previous section, the errors grow with the amplitude  $A$   
250 as expected, however, for the other parameters that define the problem the dependency is not trivial. First, a discussion on the influence of the roughness phase  $\xi$  is carried on. This is done by selecting a pair  $\lambda$ ,  $E'/p_h$ , or equivalently a pair  $M, L$  and assessing the errors in pressure and clearance, for different  $\varepsilon_0$  values and a fixed  $A_{\text{rel}} = 0.25$ . Thereafter, a sensitivity study on the errors in  
255 pressure for varying  $\lambda$  and  $E'/p_h$  is performed.



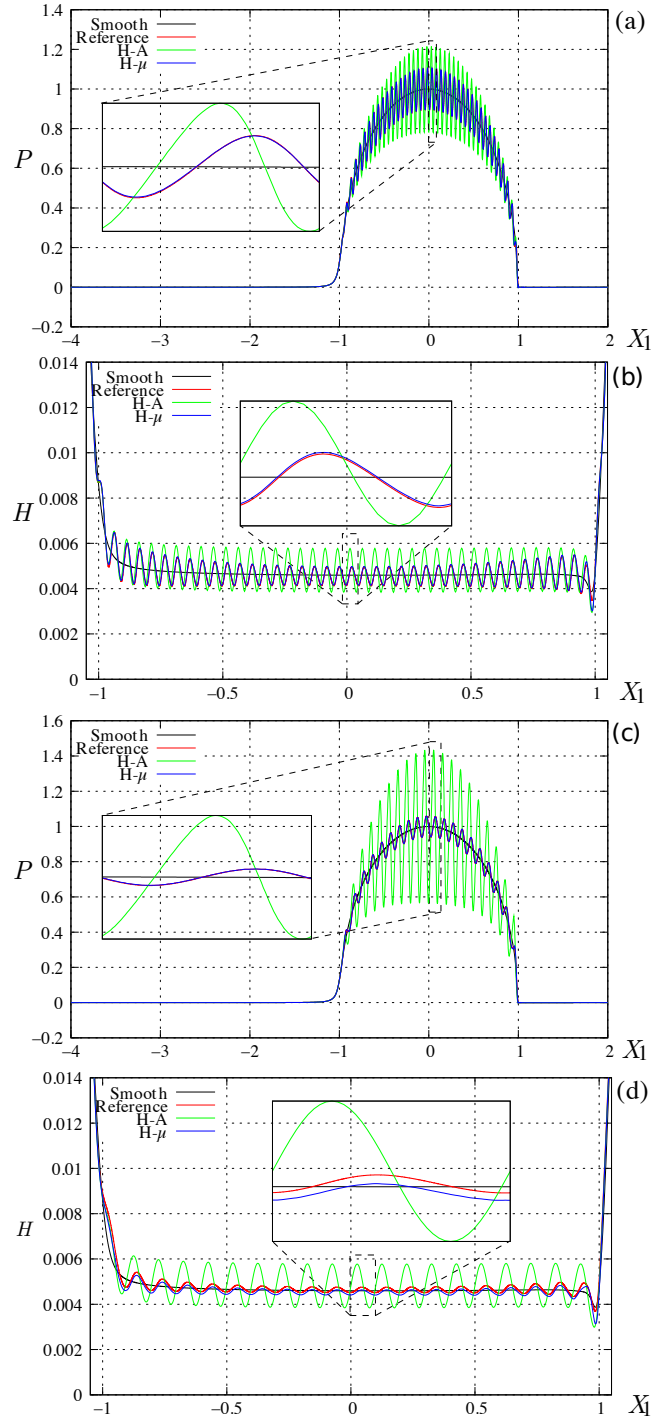


Figure 6: Pressure (a,c) and clearance (b,d) for the homogenized asymptotic (H-A) and the homogenized  $\mu$ -EHL model (H- $\mu$ ) for parameters  $M = 100$ ,  $L = 0.66$ ,  $A_{\text{rel}} = 0.25$ ,  $\varepsilon_0 = 0.05$  (top) and  $\varepsilon_0 = 0.2$  (bottom).

#### 4.2.1. Sensitivity in pressure and clearance to the phase $\xi$

The feeding conditions at the entrance of the lubricated contact are determined by the relative position of the roughness to it. This has a particular impact on the clearance, as shown in an extensive study in EHL line contacts in [35]. This effect is controlled by the deformation of the roughness, which is itself governed by the *generalized wavelength* (Venner et al [36])

$$V = \varepsilon_0 \frac{M^{3/4}}{L^{1/2}} \quad (70)$$

High  $V$  values lead to higher roughness deformations. This can be achieved either by a large wavelength  $\varepsilon_0$  or by a large  $\frac{M^{3/4}}{L^{1/2}}$  ratio. From the parameters in Table 1,  $M = 31.6$ ,  $L = 9.43$  attain the lowest  $V$  while  $M = 100$ ,  $L = 0.66$  the highest. Errors in pressure and clearance will be compared for this set of parameters.

Let us first look at the point  $M = 100$ ,  $L = 0.66$  from the Moes graph, for  $A_{\text{rel}} = 0.25$  and  $\varepsilon_0 = 0.05$ . Figures 7(a) and 7(b) show both the pressure and the clearance for the reference (full lines), smooth and the homogenized  $\mu$ -EHL (dashed lines) solutions for several phase values of  $\xi = 0, 0.25, 0.5$  and  $0.75$ . Curves computed for the same phase  $\xi$  appear in the same color. In order to compute a representative error for the clearance  $H$ , we restricted  $e_H$  to the interval  $[-1, 1]$  in all cases. The approximation both in clearance and pressure for all phases  $\xi$  is excellent, the maximum errors being  $e_P = 0.37\%$  and  $e_H = 1.13\%$ .

If the roughness wavelength is increased to  $\varepsilon_0 = 0.1$  we have the results of Figures 7(c) and 7(d). The maximum and minimum errors in pressure are  $e_P = 0.35\%$  and  $e_P = 0.29\%$  respectively. This can be seen in Figure 7(c): for each reference solution there is a closely matching homogenized pressure curve computed for the same  $\xi$  value. However, this is not the case for the clearance curves. The ones corresponding to the reference solution in Figure 7(d) present some dispersion while the  $\mu$ -EHL ones are clustered around an average, the maximum error being  $e_H = 4.2\%$  and the minimum  $e_H = 1.8\%$ .

This behavior can be explained in the following manner: the averages taken

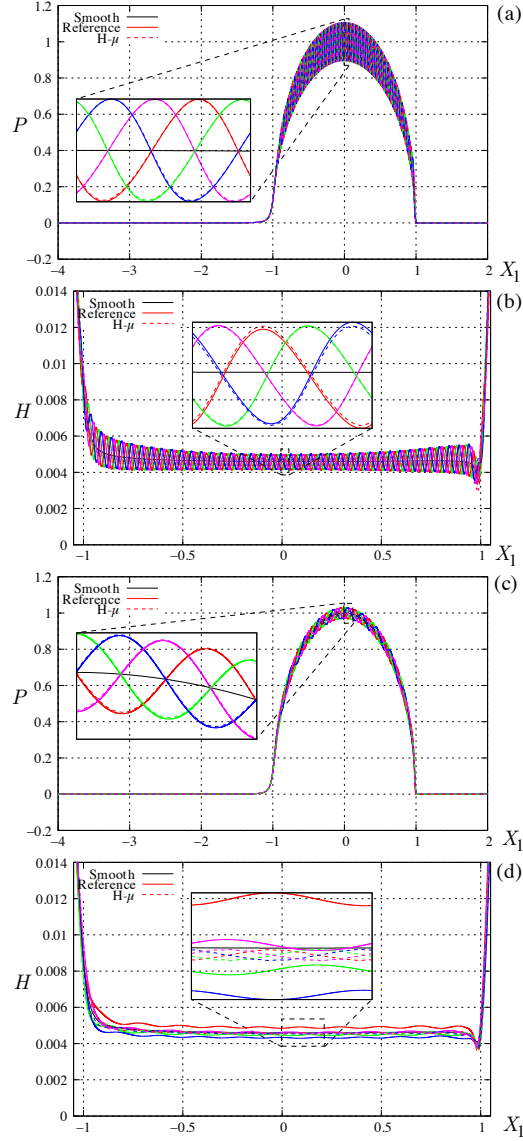


Figure 7: Pressure (a,c) and clearance (b,d) for the homogenized  $\mu$ -EHL model (dashed lines) and the reference solution (full lines) for parameters  $M = 100$ ,  $L = 0.66$ ,  $A_{rel} = 0.25$ ,  $\varepsilon_0 = 0.05$  (top) and  $\varepsilon_0 = 0.1$  (bottom). Solutions were computed for phase  $\xi$  values of 0, 0.25, 0.5 and 0.75.

280 with respect to the fast variable  $Y_1$  in order to develop the homogenized macroscopic equations induce an independency on the macroscopic quantities on the roughness phase  $\xi$ . Hence, the average values of pressure ( $P_0$ ) and clearance ( $\tilde{H}$ ) are insensitive to the phase. No significant differences are seen in pressure due to the restriction imposed by the load balance equation, which sets the average value of the pressure in each periodic cell. However, there is no equivalent  
 285 restriction for the clearance.

Let us turn now to the results for  $M = 31.6$ ,  $L = 9.43$  which are shown in Figure 8. For the sake of clarity, only the solution for  $\xi = 0$  is shown in pressure. Figures 8-(a) and 8-(b) depict the results for  $\varepsilon_0 = 0.05$ . An excellent  
 290 approximation can be seen in both pressure and clearance. The maximum error in pressure for the phases computed is  $e_P = 2.3\%$ , while it is  $e_H = 1.5\%$  in clearance. The differences between the homogenized  $\mu$ -EHL curves and the reference ones are small and limited to the inlet and outlet regions in the case of the pressure curves. Notice how in every case the micro-elastohydrodynamic  
 295 behavior is captured by the homogenized model. If we turn now to figures 8-(c) and 8-(d) we can see again an excellent fit on the pressure (maximum  $e_P = 2.5\%$ ) while some small differences are seen in the clearance curves, with a maximum error  $e_H = 2.2\%$ . These results, that of a higher error in clearance with larger deformations (larger  $V$ ) correlate well with the results of Couhier  
 300 [35] and Venner [36]. It is to be noticed that the errors  $e_P$  and  $e_H$  are more sensitive to  $\varepsilon_0$  than to  $M$  and  $L$ .

#### 4.2.2. Pressure sensitivity to $\lambda$ and $E'/p_h$

What remains to be appraised is the sensitivity on the pressure to the two main non-dimensional parameters controlling the problem:  $\lambda$  and  $E'/p_h$ . In  
 305 order to do that, the phase and amplitude are fixed to  $\xi = 0$  and  $A_{\text{rel}} = 0.25$ .

We set fixed values of  $\lambda = 3.7 \times 10^{-4}$  ( $M = 100$ ) and  $\lambda = 3.7 \times 10^{-3}$  ( $M = 31.6$ ) and vary  $E'/p_h$ . Table 3-(a) shows that for a lower  $\lambda$  value, errors slightly increase when decreasing  $E'/p_h$ . The sensitivity increases with larger  $\lambda$  values, as can be seen in a comparison between Tables 3-(a) and (a'). The

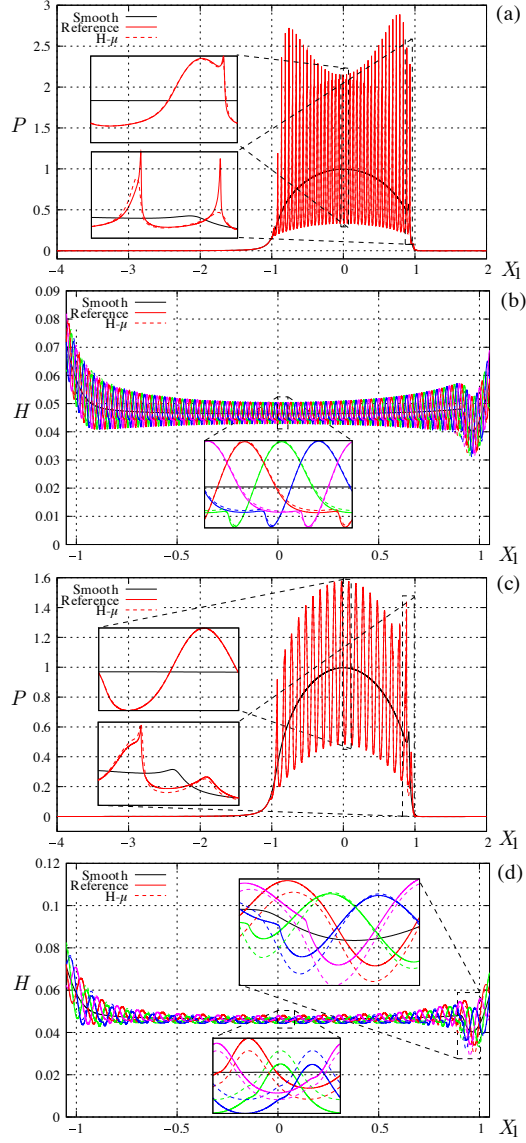


Figure 8: Pressure (a,c) and clearance (b,d) for the homogenized  $\mu$ -EHL model (do) and the reference solution for parameters  $M = 31.6$ ,  $L = 9.43$ ,  $A_{\text{rel}} = 0.25$ ,  $\varepsilon_0 = 0.05$  (top) and  $\varepsilon_0 = 0.1$  (bottom). Solutions were computed for phase  $\xi$  values of 0, 0.25, 0.5 and 0.75. For simplicity, the pressure curves are shown only for  $\xi = 0$ .

310 largest errors in pressure, which remain lower than 3%, take place for larger  $\lambda$   
and lower  $E'/p_h$  values. It is worthy of note the low sensitivity to the roughness  
wavelength, at least for the range of  $\varepsilon_0$  values analyzed here.

If  $E'/p_h$  is fixed at values of 400 and 50 and  $\lambda$  varies, we have the results of  
Table 4. Table 4-(a) shows that errors stay below 0.5% for  $E'/p_h = 400$ , and  
315 that they are quite insensitive to  $\varepsilon_0$ . A higher sensitivity is seen for  $E'/p_h = 50$   
(Table 4-(a')), as errors marginally increase with  $\varepsilon_0$ . In summary, it can be  
stated that errors are low for higher  $E'/p_h$  ratios and lower  $\lambda$  values and almost  
insensitive to  $\varepsilon_0$ , while somewhat larger for lower  $E'/p_h$  and higher  $\lambda$ .

## 5. Conclusions

320 A new homogenized approximation of the rough elastohydrodynamic lubri-  
cation problem was presented. This new approximation takes into account the  
effects of a non-negligible microscopic pressure, compared to the classical peri-  
odic asymptotic homogenization where these are neglected. As a result of this  
assumption local deformations must be computed in the microscopic periodic  
325 cells as well as the effects of the local pressure in density and viscosity. These  
are the main differences with the asymptotic approach. This allows to extend  
the applicability of homogenization methods to more realistic conditions.

The differences of the solutions obtained with the new homogenized model  
and the solution of the reference problem were assessed in parametric stud-  
330 ies. Errors in pressure are below or equal to 2% and remarkably insensitive to  
the roughness amplitude and wavelength for a wide range of Moes parameters,  
namely for  $L < 6$ . Errors in pressure grow and are slightly more sensitive to  
the amplitude of the roughness and the roughness wavelength when  $L > 6$ , but  
remain below 3% for the range  $31.6 \leq M \leq 100$ ,  $0.66 \leq L \leq 10$ .

335 Errors in clearance grow with larger  $M$  and lower  $L$  values but remain be-  
low 5%, that is with larger micro-deformations. They are more sensitive to  
the roughness wavelength than to  $M$ ,  $L$ . Micro-elastohydrodynamic effects are  
correctly captured by the newly developed homogenized method.

(a) Percentage errors for  $\lambda = 3.7 \times 10^{-4}$ 

		$E'/p_h$				
		400	200	100	50	26.5
$\varepsilon_0$	0.05	0.36	0.41	0.52	0.90	1.41
	0.1	0.29	0.37	0.43	1.12	1.52
	0.2	0.30	0.25	0.39	0.88	1.40

(b) Moes parameters

$E'/p_h$	400	200	100	50	26.5
$M$	100	100	100	100	100
$L$	0.66	1.33	2.65	5.3	10

(a') Percentage errors for  $\lambda = 3.7 \times 10^{-3}$ 

		$E'/p_h$			
		400	200	100	50
$\varepsilon_0$	0.05	0.28	0.38	1.07	2.15
	0.1	0.80	1.00	1.16	2.44
	0.2	1.06	1.64	2.01	2.63

(b') Moes parameters

$E'/p_h$	400	200	100	50
$M$	31.6	31.6	31.6	31.6
$L$	1.18	2.36	4.72	9.43

Table 3: (a, a') Percentage errors in pressure  $e_p$  relative to the reference solution for varying  $E'/p_h$  values and fixed  $\lambda$  values. The amplitude  $A_{\text{rel}} = 0.25$  in all cases. (b,b') Moes parameters for the cases of Tables (a,a').

(a) Percentage errors for $E'/p_h = 400$			
	$\lambda$		
$\varepsilon_0$	$3.7 \times 10^{-4}$	$9.25 \times 10^{-4}$	$3.7 \times 10^{-3}$
0.05	0.36	0.28	0.39
0.1	0.29	0.80	0.60
0.2	0.30	1.06	0.52

(b) Moes parameters			
$\lambda$	$3.7 \times 10^{-4}$	$9.25 \times 10^{-4}$	$3.7 \times 10^{-3}$
$M$	100	63.25	31.6
$L$	0.66	0.83	1.18

(a') Percentage errors for $E'/p_h = 50$			
	$\lambda$		
$\varepsilon_0$	$3.7 \times 10^{-4}$	$9.25 \times 10^{-4}$	$3.7 \times 10^{-3}$
0.05	0.90	1.38	2.15
0.1	1.12	1.10	2.44
0.2	0.88	1.22	2.63

(b') Moes parameters			
$\lambda$	$3.7 \times 10^{-4}$	$9.25 \times 10^{-4}$	$3.7 \times 10^{-3}$
$M$	100	63.26	31.63
$L$	5.30	6.67	9.43

Table 4: (a,a') Percentage errors in pressure  $e_p$  relative to the reference solution for varying  $\lambda$  values and fixed  $E'/p_h$  values. The amplitude  $A_{\text{rel}} = 0.25$  in all cases. (b,b') Moes parameters for the cases of Tables (a,a').



The model here presented was restricted to the one-dimensional case and  
340 stationary conditions in order to better assess its efficiency. The extension to  
the two-dimensional case and transient conditions will be the object of future  
research.

## References

- [1] S. Pei, H. Xu, F. Shi, A deterministic multiscale computation method  
345 for rough surface lubrication, *Tribology International* 94 (2016) 502–508.  
doi:10.1016/j.triboint.2015.10.005.
- [2] D. Gropper, L. Wang, T. J. Harvey, Hydrodynamic lubrication of textured  
surfaces: A review of modeling techniques and key findings, *Tribology In-*  
*ternational* 94 (2016) 509–529. doi:10.1016/j.triboint.2015.10.009.
- 350 [3] J. Raisin, N. Fillot, D. Dureisseix, P. Vergne, V. Lacour, Characteristic  
times in transient thermal elastohydrodynamic line contacts, *Tribology In-*  
*ternational* 82 (2015) 472–483. doi:10.1016/j.triboint.2014.02.022.
- [4] F. Sadeghi, P. C. Sui, Thermal elastohydrodynamic lubrication of  
rolling/sliding contacts, *Journal of Tribology* 112 (2) (1990) 189–195.  
355 doi:10.1115/1.2920241.
- [5] L. Chang, Traction in thermal elastohydrodynamic lubrication of rough sur-  
faces, *Journal of tribology* 114 (1) (1992) 186–191. doi:10.1115/1.2920859.
- [6] J. Wang, M. Kaneta, A study on starved micro-thermal elastohydrody-  
namic lubrication in simple sliding circular contacts, *Proceedings of the*  
360 *Institution of Mechanical Engineers, Part J: Journal of Engineering Tribol-*  
*ogy* 221 (3) (2007) 209–221. doi:10.1243/13506501JET223.
- [7] J. Wang, A. A. Lubrecht, P. Sperka, M. Omasta, M. Kaneta, Effect of high  
slide-roll ratio on thermal elastohydrodynamic lubrication in line contacts

- with surface waviness, *Proceedings of the Institution of Mechanical Engineers, Part J: Journal of Engineering Tribology* 229 (5) (2015) 568–577. doi:10.1177/1350650114556397.
- [8] C. J. Hooke, The behaviour of low-amplitude surface roughness under line contacts, *Proceedings of the Institution of Mechanical Engineers, Part J: Journal of Engineering Tribology* 213 (4) (1999) 275–285. doi:10.1243/1350650991542668.
- [9] G. E. Morales-Espejel, V. Brizmer, E. Piras, Roughness evolution in mixed lubrication condition due to mild wear, *Proceedings of the Institution of Mechanical Engineers, Part J: Journal of Engineering Tribology* 229 (11) (2015) 1330–1346. doi:10.1177/1350650115577404.
- [10] X. Wang, Y. Liu, D. Zhu, Numerical solution of mixed thermal elastohydrodynamic lubrication in point contacts with three-dimensional surface roughness, *Journal of Tribology* 139 (1) (2017) 011501. doi:10.1115/1.4032963.
- [11] D. Zhu, J. Wang, Q. J. Wang, On the Stribeck curves for lubricated counterformal contacts of rough surfaces, *Journal of Tribology* 137 (2) (2015) 021501. doi:10.1115/1.4028881.
- [12] A. Akchurin, R. Bosman, P. Lugt, M. van Drogen, On a model for the prediction of the friction coefficient in mixed lubrication based on a load-sharing concept with measured surface roughness, *Tribology letters* 59 (1) (2015) 19. doi:10.1007/s11249-015-0536-z.
- [13] W. Pu, J. Wang, D. Zhu, Friction and flash temperature prediction of mixed lubrication in elliptical contacts with arbitrary velocity vector, *Tribology International* 99 (2016) 38–46. doi:10.1016/j.triboint.2016.03.017.
- [14] D. Zhu, H. S. Cheng, T. Arai, K. Hamai, A numerical analysis for piston skirts in mixed lubrication Part I: Basic modeling, *Journal of tribology* 114 (3) (1992) 553–562. doi:10.1115/1.2920917.

- [15] N. Patir, H. S. Cheng, An average flow model for determining effects of three-dimensional roughness on partial hydrodynamic lubrication, *Journal of Lubrication Technology* 100 (1) (1978) 12–17. doi:10.1115/1.3453103.
- 395 [16] M. Masjedi, M. Khonsari, On the effect of surface roughness in point-contact EHL: Formulas for film thickness and asperity load, *Tribology International* 82 (2015) 228–244. doi:10.1016/j.triboint.2014.09.010.
- [17] R. Larsson, Modelling the effect of surface roughness on lubrication in all regimes, *Tribology International* 42 (4) (2009) 512–516.  
400 doi:10.1016/j.triboint.2008.07.007.
- [18] G. Bayada, Application of the homogenization method to Reynolds roughness, in: *Developments in Numerical and Experimental Methods Applied to Tribology: Proceedings of the 10th Leeds–Lyon Symposium on Tribology*, Elsevier, 2014, p. 53.
- 405 [19] G. Bayada, S. Martin, C. Vázquez, Homogenization of a nonlocal elastohydrodynamic lubrication problem: a new free boundary model, *Mathematical Models and Methods in Applied Sciences* 15 (12) (2005) 1923–1956. doi:10.1142/S0218202505001023.
- [20] G. Bayada, S. Martin, C. Vázquez, Micro-roughness effects in  
410 (elasto)hydrodynamic lubrication including a mass-flow preserving cavitation model, *Tribology International* 39 (2006) 1707–1718. doi:10.1016/j.triboint.2006.03.003.
- [21] C. H. Venner, A. A. Lubrecht, An engineering tool for the quantitative prediction of general roughness deformation in EHL contacts based on harmonic waviness attenuation, *Proceedings of the Institution of Mechanical Engineers, Part J: Journal of Engineering Tribology* 219 (5) (2005) 303–312.  
415 doi:10.1243/135065005X33973.
- [22] M. Budt, I. Temizer, P. Wriggers, A computational homogenization frame-

- work for soft elastohydrodynamic lubrication, *Computational Mechanics* 49 (6) (2012) 749–767. doi:10.1007/s00466-012-0709-7.
- 420 [23] T. W. Kim, Y. J. Cho, The flow factors considering the elastic deformation for the rough surface with a non-Gaussian height distribution, *Tribology Transactions* 51 (2) (2008) 213–220. doi:10.1080/10402000701730502.
- [24] F. Sahlin, R. Larsson, A. Almqvist, P. M. Lugt, P. Marklund, A mixed lu-  
425 brication model incorporating measured surface topography. Part 1: The-  
ory of flow factors, *Proceedings of the Institution of Mechanical Engi-  
neers, Part J: Journal of Engineering Tribology* 224 (4) (2009) 335–351.  
doi:10.1243/13506501jet658.
- [25] M. Scaraggi, G. Carbone, B. N. J. Persson, D. Dini, Lubrication in soft  
430 rough contacts: A novel homogenized approach. Part I-Theory, *Soft Matter*  
7 (21) (2011) 10395–10406. doi:10.1039/C1SM05129F.
- [26] M. Scaraggi, L. Dorogin, J. Angerhausen, H. Murrenhoff, B. N. J. Pers-  
son, Elastohydrodynamics for soft solids with surface roughness: Transient  
effects, *Tribology Letters* 65 (3) (2017) 95. doi:10.1007/s11249-017-0878-9.
- 435 [27] W. Habchi, D. Eyheramendy, P. Vergne, G. Morales-Espejel, Sta-  
bilized fully-coupled finite elements for elastohydrodynamic lubrica-  
tion problems, *Advances in Engineering Software* 46 (1) (2012) 4–18.  
doi:10.1016/j.advengsoft.2010.09.010.
- [28] B. Hamrock, S. Schmid, B. Jacobson, *Fundamentals of fluid film lubrica-  
440 tion*, Marcel Dekker, New York, 2004. doi:10.1201/9780203021187.
- [29] K. L. Johnson, *Contact Mechanics*, Cambridge University Press, 1987.
- [30] D. Dowson, G. R. Higginson, *Elasto-hydrodynamic lubrication*, Interna-  
tional series on materials science and technology, Pergamon Press, 1977.  
doi:10.1016/C2013-0-05764-7.

- 445 [31] C. J. A. Roelands, Correlational Aspects of the Viscosity-temperature-pressure Relationships of Lubricating Oils, Druk. V.R.B., 1966.
- [32] J. Davim, Tribology in manufacturing technology, Springer, 2012.
- [33] C. H. Venner, Multilevel Solution of the EHL Line and Point Contact Problems, 1991.
- 450 [34] F. Feyel, J. L. Chaboche, Multi-scale non-linear FE2 analysis of composite structures: damage and fiber size effects, *Revue Européenne des Éléments Finis* 10 (2-4) (2001) 449–472. doi:10.1080/12506559.2001.11869262.
- [35] F. Couhier, Influence des rugosités de surface sur les mécanismes de lubrification du contact élastohydrodynamique cylindre-plan, Ph.d. thesis, INSA  
455 Lyon (1996).
- [36] C. H. Venner, F. Couhier, A. A. Lubrecht, J. A. Greenwood, Amplitude reduction of waviness in transient EHL line contacts, in: *Tribology Series*, Vol. 32, Elsevier, 1997, pp. 103–112. doi:10.1016/S0167-8922(08)70440-1.